Wind and Structures, *Vol. 21, No. 3 (2015) 331-352*
DOI: http://dx.doi.org/10.12989/was.2015.21.3.331

Aerodynamic measurements of across-wind loads and responses of tapered super high-rise buildings

Ting Deng, Xianfeng Yu and Zhuangning Xie*

School of Civil Engineering and Transportation, State Key Laboratory of Subtropical Building Science, South China University of Technology, Guangzhou 510640, China

(Received December 29, 2014, Revised August 25, 2015, Accepted September 1, 2015)

Abstract. A series of wind tunnel tests were conducted on tapered super high-rise buildings with a square cross section by applying synchronous pressure measurement technology. The effects of global strategy of chamfered modification on aerodynamic loads and wind-induced responses were investigated. Moreover, local aerodynamic strategies of opening a ventilation slot in the corner of equipment and refuge floors were carried out. Results show that the global strategy of tapered elevation increased the vortex shedding frequency, but reduced vortex shedding energy, leading to reduction of across-wind aerodynamic loads and responses. Chamfered modification suppressed the across-wind vortex shedding effect on tapered buildings. Opening the ventilation slot further suppressed the strength of vortex shedding and reduced the residual energy related to vortex shedding in aerodynamic loads of chamfered buildings. Finally, the optimized locations of local aerodynamic strategies were suggested.

Keywords: super high-rise building; chamfered modification; local aerodynamic strategy; vortex shedding; remaining spectral energy

1. Introduction

In recent years, with the economic development, more and more super high-rise buildings with heights of 400 to 800 m are under construction, or have been built. These buildings have become increasingly sensitive to wind loads, with an increase in height and flexibility, and with a decrease in damping. For super high-rise buildings with heights of over 400 to 600 m, across-wind loads and responses are among the most significant factors determining the structural safety and comfort to the occupants. Aerodynamic shape plays an important role in controlling across-wind loads. Appropriate building shape, determined by aerodynamic optimal design, can effectively reduce across-wind loads and responses (Tanaka *et al*. 2012, Xie 2014). The optimum designs of aerodynamic shapes usually include both global and local strategies.

Global strategies, such as an appropriate building cross section, changing the cross-section by tapering or setback, as well as corner modification, have been widely investigated. Hayashida and Iwasa (1990) examined the aerodynamic characteristics of tall buildings with different cross sections. It was found that the aerodynamic performance of a building with a square section was

*Corresponding author, Professor, E-mail: znxie@scut.edu.cn

http://www.techno-press.org/?journal=was&subpage=8 ISSN: 1226-6116 (Print), 1598-6225 (Online)

the worst. Through a wind tunnel test of aeroelastic models, Kawai (1998) discussed the effects of three kinds of corner modification, namely, corner cut, roundness, and recession on reducing across-wind response of a high-rise building with square cross-section. He drew the conclusion that the corner roundness was most effective to suppress the aeroelastic instability for a square prism. Tamura and Miyagi (1999) experimentally investigated the effects of corner shape and turbulence intensity of approaching wind on the averaged and fluctuating values of lift and drag forces. Kim and You (2002, 2008) studied across-wind responses of tapered high-rise buildings with height of 160 m through wind tunnel tests on rigid and aeroelastic models and then compared the results with those with square cross-sections. Their results showed that the global strategy of adopting tapered building facade could significantly reduce wind-induced excitations on tall buildings. However, the wind-induced responses of buildings with large taper ratio would be stronger than those with a standard square cross-section at a low damping ratio. Gu and Quan (2004) analyzed 15 typical high-rise buildings with various cross-sections. The effects of different aspect ratios, side ratios, and corner modifications on the base overturning moment were discussed in detail. They showed that corner modifications on buildings, such as chamfered and cut corners, could effectively suppress wind-induced responses. Kim and Kanda (2010, 2015) investigated the aerodynamic forces, pressures, the characteristics of overturning moments and wind-induced responses of tapering and building models with set-backs, under suburban and urban flow. Tanaka *et al*. (2012) examined the aerodynamic forces and wind pressures acting on tall buildings with various unconventional configurations. Bandi *et al*. (2013) studied aerodynamic modifications with cut corner and helical shape through a wind tunnel test and demonstrated that helical buildings had remarkable influence on aerodynamic characteristics. Kim *et al.* (2015) investigated the effect of taper on fundamental aeroelastic behaviors in three incident flows. Results showed that the suppression of responses by introducing taper was profound in the low-turbulence flow and boundary-layer flow, but the response become larger than that of the square model in the grid-generated flow. Aerodynamically efficient plan shapes were shown to be an effective means of suppressing wind-induced loads, and hence construction cost, but might come at the cost of reducing both the size and value of saleable/rentable floor area. The impact and value of aerodynamic modifications, based on wind engineering considerations, on the building economics of tall structures, have been investigated by Tse *et al*. (2009).

Opening ventilation slots or holes on buildings are usually classified into local aerodynamic strategies. Based on high frequency force balance technique, Miyashita and Katagiri (1993) examined the aerodynamic characteristics of square-shape tall buildings with corner cutting or opening holes. Results showed that opening holes could decrease wind-induced responses at a certain degree. To *et al*. (2012) studied the effect of a through-building gap on wind-induced loads and dynamic responses of a tall building. They showed that both configurations of a through-building gap were effective in reducing the cross-wind excitation with the one with opening around the perimeter of the floor being significantly more effective, and that the through-building gap reduced the fluctuating across-wind forces, through a disturbance of the coherence and phase-alignment of vortex excitation.

These research results above mostly focus on the super high-rise buildings with heights of below 400 m, and the conclusions can not necessarily been applied to the super high-rise buildings with heights of over 400 m. Moreover, those aerodynamic measurements also mostly focussed on aerodynamic characteristics of various types of tall buildings with different configurations. However, few studies simultaneously involve tapering and corner modification of the cross-section. Furthermore, the mitigation effects of opening ventilation slot or holes on vibration, after changing

the cross-section by tapering or corner modification have seldom been studied. Therefore, in the present study, wind tunnel tests on rigid tapered super-high-rise building models with square cross-sections were primarily conducted to examine the effects of global strategy of chamfered modification. On the basis of global strategy, the local strategy of opening ventilation slot in the corner of equipment and refuge floors was studied. Subsequently, the effects of different aerodynamic measurements on local across-wind aerodynamic loads, base overturning moment, and dynamic responses were analyzed in detail. Moreover, the effects of structural modal parameters on peak dynamic base overturning moment are also discussed in this paper. Finally, the intrinsic laws in the influence of various aerodynamic measurements on across-wind loads and responses are given. The engineering applicability of aerodynamic measurements is also discussed.

2. Outline of wind tunnel experiments

2.1 Experimental conditions

Wind tunnel tests were performed in the STDX-1 boundary layer wind tunnel at Shantou University. A test section of the wind tunnel with 3 m width, 2 m height, and 20 m length was utilized. The height of the buildings is 546 m, which is higher than the gradient height stipulated in the load code for the design of building structures in China. The wind field was simulated to match data of the ESDU (Engineering Science Data Unit), one which is frequently used in international wind engineering. The simulated profiles of mean wind speed and turbulence intensity in suburban terrain are plotted in Fig. 1. Wind velocity and turbulence intensity at the top of the model were about 12.1 m/s and 8.8%, respectively. Fig. 2 presents the power spectral density (PSD) of the approaching flow at the top of the buildings, which is consistent with Karman spectrum. The turbulence integral scale near the top of the buildings was 380 m. Fig. 3 plots the definitions of wind forces and coordinate system adopted for the calculations, where β is the wind direction angle.

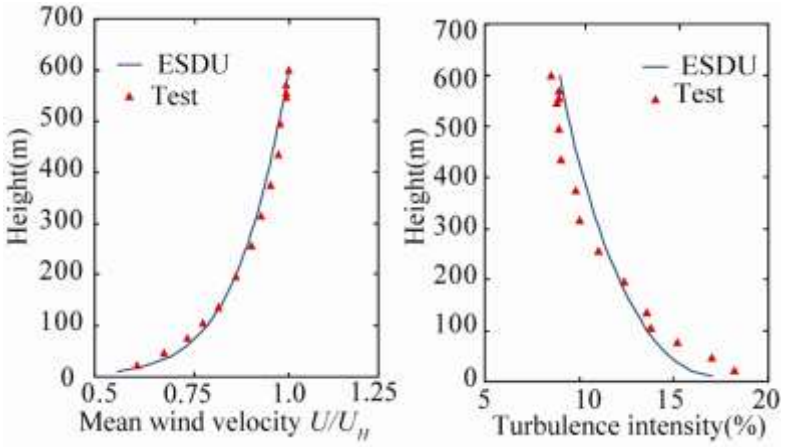

Fig. 1 Simulated wind parameters in wind tunnel

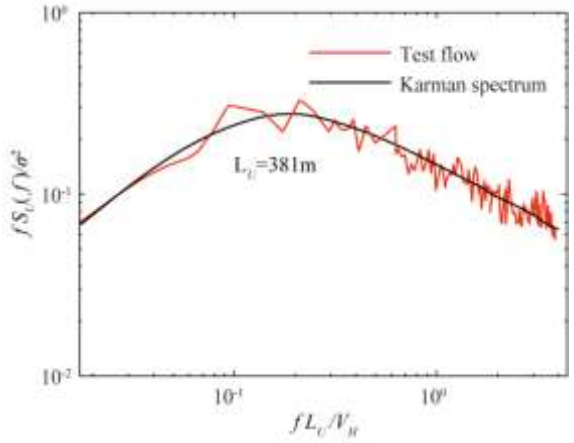

Fig. 2 PSD of approaching flow at the top of the building

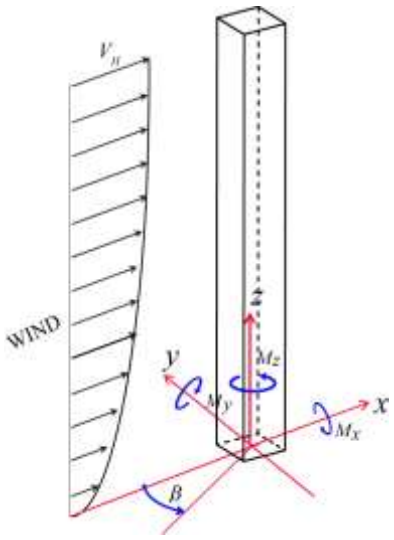

Fig. 3 Definition of coordinate system

2.2 Configurations of building models

The dimensions of seven test models (A, B, C, D, E, F, and G) are shown in Fig. 4. The length scale was set at a ratio of 1: 600. Each of the full-scale buildings has a breadth of B = 60 m and a height of H = 546 m. The shape and structural dynamic parameters are given in Table 1. Model A is the building with a standard square cross section without tapering, whereas models C, E, and G are buildings with a square cross section that change in height through tapering. In this paper, the taper ratio η is defined by: $\eta = \frac{B_{bottom}-B_{top}}{H} \times 100\%$, where B_{bottom}, B_{top}, H are the width at bottom, width at top and height of buildings. The taper ratios (η) of models C, E, and G are 2.2%,

4.4%, and 6.6%, respectively. The global strategy of chamfered modification was applied to on models B, D, and F based on models A, C, and E with a cut size of 3 m. The pressure taps were installed in 14 levels of all the buildings with various heights. There were about 30 pressure taps on each level, and more taps were placed near the corner of cross section to capture negative pressures characterized by flow separation on the side faces. The locations of the pressure taps that were denoted by tap name and lay number (1-14) are shown in Fig. 5. The fluctuating wind pressure of the tap was measuring by a digital service module at a sampling frequency of 312.5Hz. The length of pressure tubing was set to the same to minimize the influence of tubing response. All pressure values were measured relative to undistributed ambient pressure in the wind tunnel as measured by the pitot-static tube. Moreover, local aerodynamic strategies were adopted in model A, B, C, and D. The local strategy shown in Fig. 6 shows the opening ventilation slot in the corner of equipment and refuge floors, so that wind can freely flow through it. The ventilation slots were 10.8 m in width; 10.8 m in length; and 9 m in height, which were inserted in the buildings with heights of: 450 m, 330 m, and 210 m. They are expressed by S1, S2, and S3 in Fig. 5. The ventilation slots were inserted when the models were completed. Plastic blocks matching the ventilation slots were also made. The ventilation slots were closed if plastic blocks were placed on the buildings; on the contrary, the ventilation slots were open if plastic blocks were removed from the buildings. The test cases of opening all ventilation slots, closing all ventilation slots, and opening each ventilation slot were considered in the current study. Fig. 7 shows the models in the wind tunnel test.

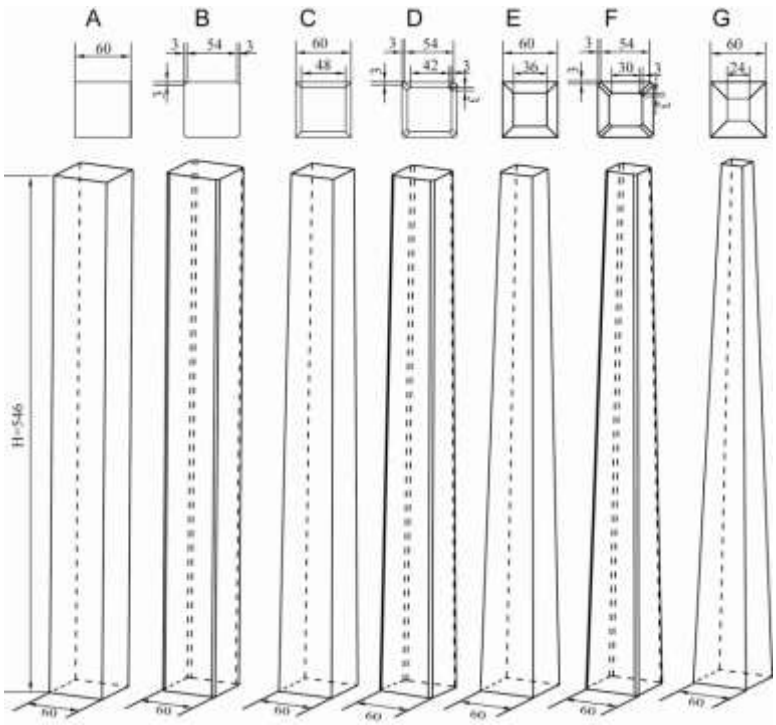

Fig. 4 Dimensions of each model (unit: m)

Table 1 Shape parameters and structural dynamic parameters of test buildings

		Width at the top (m)	Width at the bottom (m)	Height (m)	Natural frequency (Hz)	Damping ratio (%)
Model I	A	60	60	546	0.098	2.0
	B	54 (chamfer)	54 (chamfer)	546	0.098	2.0
Model II	C	48	60	546	0.098	2.0
	D	42 (chamfer)	54 (chamfer)	546	0.098	2.0
Model III	E	36	60	546	0.098	2.0
	F	30 (chamfer)	54 (chamfer)	546	0.098	2.0
Model IV	G	24	60	546	0.098	2.0

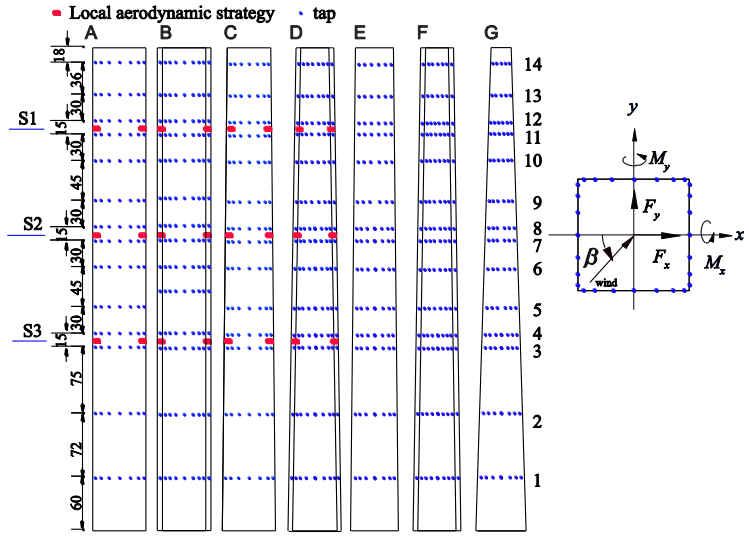

Fig. 5 Pressure taps installed on models (unit: m)

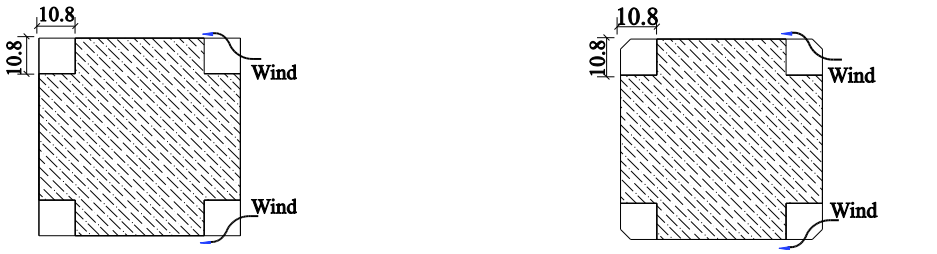

(a) models with square cross-section (b) models with chamfer modification

Fig. 6 Schematic plan of local aerodynamic strategies. (unit: m)

Fig. 7 Building model in wind tunnel

2.3 Data processing methods

The wind pressure time history $p(t)$ of pressure tap can be obtained through wind tunnel tests; and the local aerodynamic loads at unit height is calculated by integration as follows

$$F(t) = \int_L p(t)\cos\alpha_L dL \tag{1}$$

where L is the contour curve of buildings at the height of the pressure tap levels, α_L is the angle between the contour curve and x or y axis.

The coherence function γ (defined as a function of distance Δz and frequency *f*), which indicates the correlation of aerodynamic loads in frequency domain, can further reveal the mechanism of aerodynamic strategy and is defined as

$$\gamma(\Delta z, f) = \frac{\left|S_{F_iF_j}(f)\right|}{\sqrt{S_{F_i}(f)S_{F_j}(f)}} \tag{2}$$

where $S_{F_i}(f)$ and $S_{F_j}(f)$ are the PSDs of F_i and F_j, respectively; $S_{F_iF_j}(f)$ is the cross-power spectral density; Δz is the distance between two pressure tap levels; and f is the frequency.

The base overturning moment is proportional to the first-order generalized force, when it is assumed that structural mode is linearly distributed along with the height of the building. Thus, the base overturning moment obtained from the integral of aerodynamic loads along with building height is an important indicator of aerodynamic performance. The aerodynamic overturning moment M_A can be represented as

$$M_A = \int_0^H F(z) z \, \mathrm{d}z \tag{3}$$

where $F(z)$ is the local aerodynamic forces at the height *z*. Hence, the PSD of wind-induced base blending moment (BBM) can be further written as

$$S_{M_D}(f) = |H(f)|^2 S_{M_A}(f) \tag{4}$$

where $S_{M_A}(f)$ is the PSD of the base aerodynamic overturning moment M_A in Eq. (3). $|H(f)|^2$ is the mechanical admittance of building, which can be obtained as

$$|H(f)|^2 = \frac{1}{[1-(f/f_0)^2]^2 + 4\zeta^2 (f/f_0)^2} \tag{5}$$

where ζ is the modal damping ratio equal to 2.0% in the current study, and f_0 is the first-order natural frequency equal to 0.098 Hz. The peak dynamic moment can be written as

$$M_{D_{\max}} = \bar{M}_D + g\sigma_{M_D}, M_{D_{\min}} = \bar{M}_D - g\sigma_{M_D} \tag{6}$$

where $\bar{M}_D$ is the mean moment, σ_{M_D} is the standard deviation of M_D, and g is the resonant peak factor. For a Gaussian process $g = \sqrt{2\ln(f_0 T)} + 0.5772/\sqrt{2\ln(f_0 T)}$ in which T is the observation time (Davenport 1964).

3. Experimental results and discussions

3.1 Tapered models of a square cross section

The characteristics of aerodynamic wind loads and responses for tapered tall buildings with a square cross section are discussed in this section.

3.1.1 Local across-wind aerodynamic loads

The PSD of the local across-wind aerodynamic forces for square cross-sectional buildings with various taper ratios are presented for five typical representative levels in Fig. 8. A sharp peak is observed in these plots, which is induced by across-wind vortex shedding. Moreover, it is clear that the peak frequency varies slightly with the height for the model with taper ratio η = 0%. Those of model C become constant since the fourth level, model F becomes constant since the seventh level, and model G becomes constant from the tenth level. Spectral energies of across-wind aerodynamic loads reduce rapidly with increase in taper ratio η. The peak value is about 300 kN^2s/m^2 at taper ratio η = 0%, whereas it significantly drops to about 50 kN^2s/m^2 at taper ratio η = 6.6%.

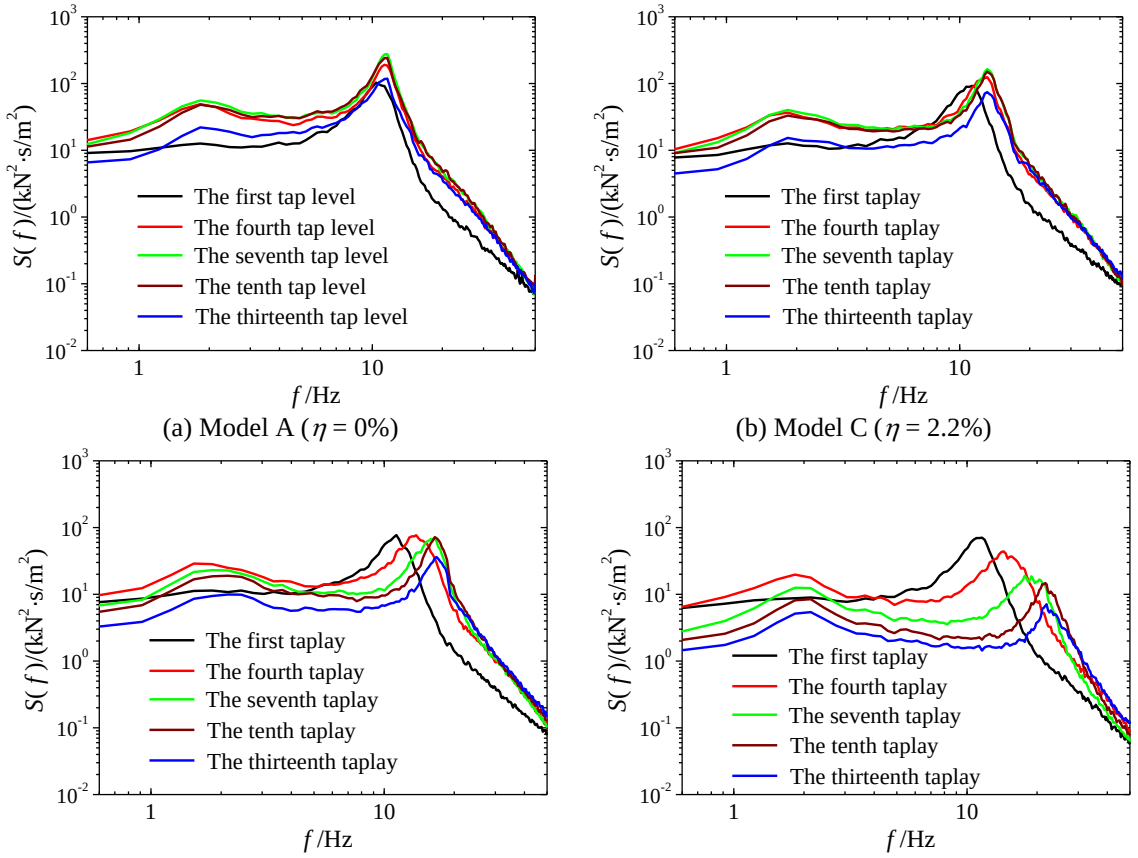

(a) Model A (η = 0%) (b) Model C (η = 2.2%)

(c) Model E (η = 4.4%) (d) Model G (η = 6.6%)

Fig. 8 Distribution of PSD of the across-wind aerodynamic force along with height

Fig. 9 presents the variation of standard deviations of local across-wind aerodynamic load (σ_{F_y}) along with the height of buildings. The value of σ_{F_y} at the same height decreases significantly with a rising taper ratio η. The maximum reduction of σ_{F_y} occurs at the upper middle of the models, but barely decreases at the bottom of the models. Moreover, the height corresponding to the maximum spectrum energy also decreases with increasing taper ratio η.

The Strouhal number (St) is obtained when the higher frequency in Fig. 8 is made dimensionless. St is written as follows

$$\mathrm{St} = f \cdot D / V_H \tag{7}$$

where V_H is the reference wind speed at the top of the building model; D is the characteristic width of the model, which is equal to 0.1 m in this paper for convenient comparison in different models. So St varies with f which is the peak frequency of PSD in Fig. 8. Fig. 10 shows the

variation of St with building height for various taper ratios. St grows with increasing taper ratio in the same building height. The Strouhal Number of model A with a standard square cross section with taper ratio η = 0% varies slightly with height, and retains an almost constant value throughout the height. Those of model C with taper η = 2.2% above 0.38 *H* are constant, model F with taper η = 4.4% is above 0.6 *H*, and model G with taper η = 6.6% is above 0.8 *H*. It is easy to know that St depends on the vortex shedding frequency through Eq. (7). For the tapered models, the vortex shedding frequencies of various tap levels depends on the breadth of buildings. The smaller the breadth is, the higher the vortex shedding frequency is. The phenomenon that the frequency is constant at a certain height range may be related to the 'lock-in' mechanism of vortex shedding. Notably, St is dependent on the characteristic width D. In this paper, D is the same for all models, which causes the values of St at the top of buildings to differ with different taper ratio models, and the values move in the range from 0.105 to 0.194. The values will change in the range from 0.105 to 0.113, if the width of buildings in two-thirds of height is utilized to calculate the Strouhal Number. For models A, C, E and G, the breadths at the two-thirds of height are 60 m, 52 m, 44 m and 36 m, respectively.

3.1.2 Base aerodynamic overturning moment and across-wind responses

Fig. 11 shows the power spectral densities of the base aerodynamic overturning moment for different tapered models. q_H is the reference overturning moment ($q = \frac{1}{2}\rho V_H^2 DH^2$), ρ is the density of air, D is the characteristic width of model (D = 0.1 m), and V_H is reference wind speed at the top of model. The prototype frequency can be converted to model frequency by $f_{\mathrm{m}} = f_{\mathrm{p}} \cdot \lambda_L / \lambda_V$, where λ_L is the length scale and λ_V is the velocity scale. Corresponding to the prototype frequency f_p = 0.098 HZ, the model frequencies corresponding to 100-year return period and 10-year return period are 12.29 Hz and 17.38 Hz, respectively. With increasing taper ratio, the peak values of the power spectral density of base aerodynamic overturning moment decreases rapidly, and the frequency corresponding to vortex shedding also increases.

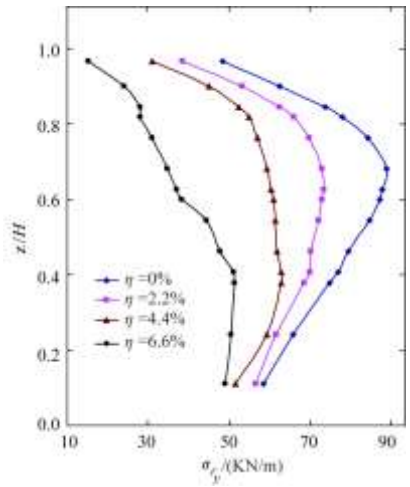

Fig. 9 Variation of standard deviation of across-wind aerodynamic forces along with building height

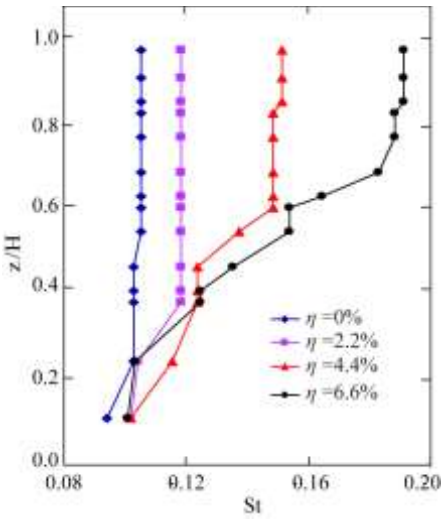

Fig. 10 Variations of St with building height for different taper ratios

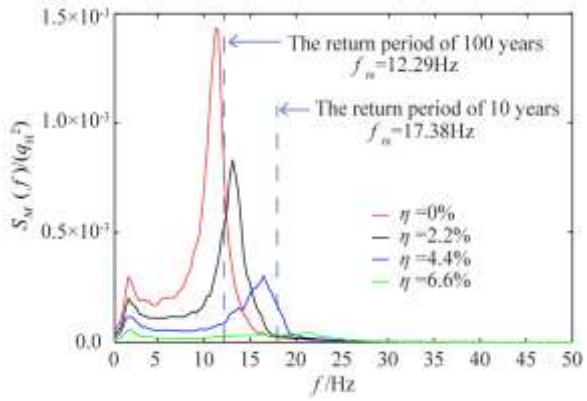

Fig. 11 PSD of across wind aerodynamic overturning moment of different taper ratio buildings

The natural periods of buildings in this paper were estimated according to the suggestions of building codes, and on existing buildings. However, actual natural frequency may vary to some extent. Consequently, to comprehensively evaluate the aerodynamic performance, it is necessary to take into account the effect of period ratio on the wind-induced response. Fig. 12 shows the variation of the peak base dynamic moment corresponding to 100-year return period with period ratio (P_r) for different tapered buildings, where P_r is defined as the ratio of natural period of building prototype to natural period adopted in current calculation. As the natural period may be uncertain at evaluation of structural parameters, it is necessary to consider the changing of the natural period over a certain range (Tamura and Suganuma 1996, Solari 1996). Besides, according to the similarity law for frequency (the reduced frequency $f_r = f \cdot D / V_H$), the reduced frequency

f_r of model is the same as that of the corresponding prototype building, so when the period of buildings is fixed, the effects of the width of buildings D and the wind velocity V_H at the top of buildings also should be considered. Taking all these into account, the range of period ratios is from 0.6 to 1.4, which is equivalent to the range of natural periods of full-scale buildings from 6.12 s to 14.28 s. As shown in Fig. 12, the shrinking of the cross section of buildings through tapering will obviously reduce the peak base dynamic moment, when the period ratio is equal to or greater than 0.9. When the period ratio is equal to 1.0, the peak base dynamic moment of buildings with taper ratio η = 2.2%, 4.4%, and 6.6% decreased by 44.12%, 68.42%, and 81.85%, respectively, in comparison with the buildings with taper ratio η = 0%. However, compared with the buildings with taper ratio η = 0%, the peak dynamic moment of the buildings with taper ratio η = 2.2% and 4.4% is greater when period ratio is less than 0.8. The minimum peak base dynamic moment occurs on the building with taper ratio η = 6.6%.

3.2 Chamfered modification

3.2.1 Local across-wind aerodynamic loads

Fig. 13 shows PSD of the local across-wind aerodynamic forces at different tap levels of chamfered buildings. Compared with the buildings without chamfered modification, the sharp peak of PSD in each building at vortex shedding frequency is suppressed after chamfered modification. It will lead to a reduction of the based overturning moment and so chamfered modification is effective in reducing the wind-induced response for buildings with square section. In order to further present the influence of chamfered modification, the standard deviation of local across-wind aerodynamic loads which reflects the total energy is shown in Fig. 14.

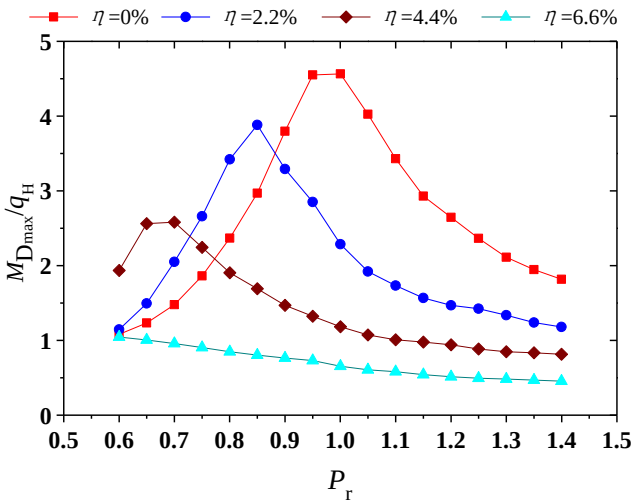

Fig. 12 Variations of peak dynamic moment with period ratios

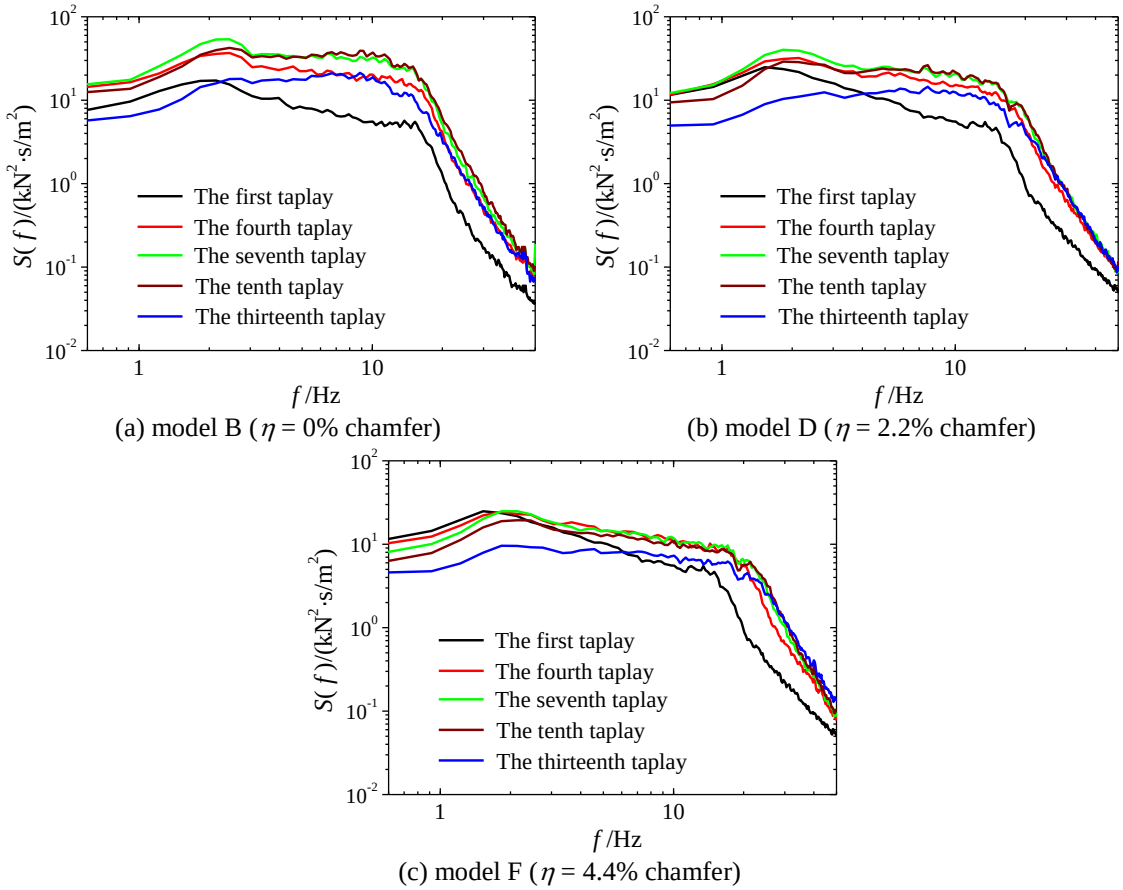

(a) model B (η = 0% chamfer) (b) model D (η = 2.2% chamfer)

(c) model F (η = 4.4% chamfer)

Fig. 13 Effects of chamfered modification on PSD of local across-wind aerodynamic load

It is obvious that the standard deviation is significantly decreased by chamfered modification. Notably, the standard deviations of local aerodynamic loads for chamfered model D (η = 2.2%, chamfered modification) are obviously less than that for model E (η = 4.4%) without chamfered modification. Moreover, standard deviations of local aerodynamic loads for chamfered model B (η = 0%, chamfered modification) are obviously less than that for model C (η = 2.2%) without chamfered modification. This indicates that the chamfered modification in reducing the local across-wind aerodynamic loads is more effective than the shrinking of cross section through tapering. Besides, larger taper ratios will not be accepted in engineering application because it will reduce the floor area. Thus, a small taper ratio and chamfered modification may be a suitable choice for wind-resistant design.

3.2.2 Base aerodynamic overturning moment

Fig. 15 shows that PSD of base aerodynamic overturning moments of chamfered models B, D, and F vary with taper ratios. In order to compare with model without chamfered modification, the

power spectral density of the base aerodynamic overturning moment of model A with a standard square cross section without taper is also plotted. The peak value of PSD for each chamfered model is much smaller than the one without chamfered modification. This is consistent with the conclusions drawn from Fig. 13.

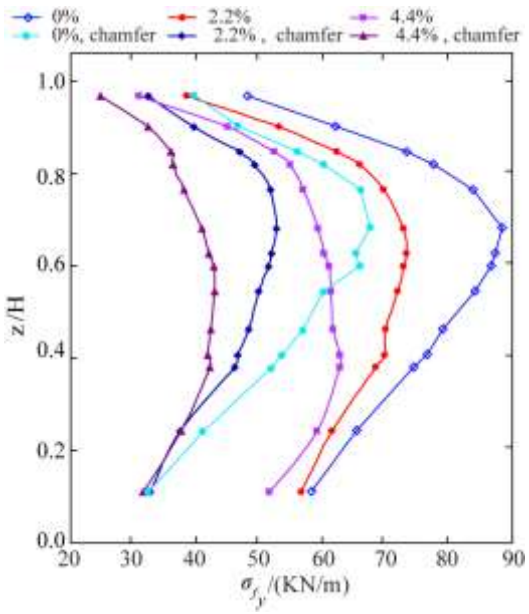

Fig. 14 Effects of chamfered modification on standard deviation of across-wind aerodynamic load in different heights

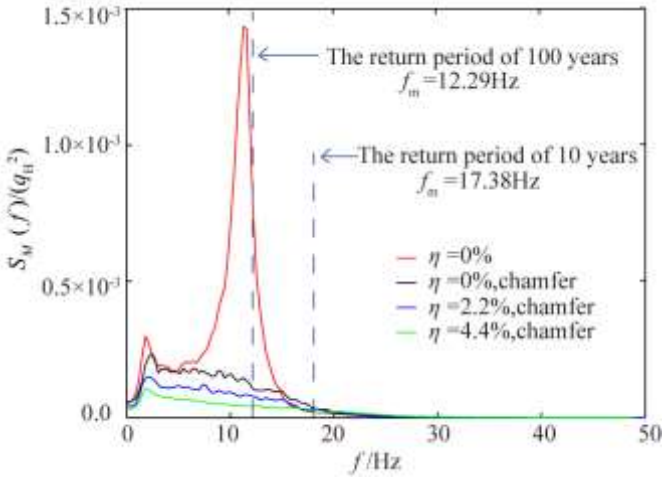

Fig. 15 Effects of chamfered modification on PSD of across-wind base aerodynamic overturning moment

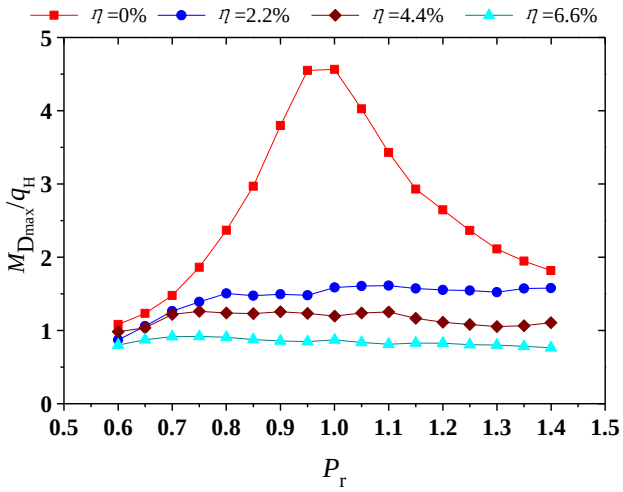

Fig. 16 Effects of chamfered modification on peak base dynamic moment for different period ratios

Fig. 16 shows variations of peak dynamic moments for three chamfered models with period ratios; and that of model A with a standard square cross section without taper is also presented. In comparison with model A, the peak dynamic moments of chamfered models with taper ratios η = 0%, 2.2%, and 4.4% reduce by 65.25%, 73.81%, and 80.93%, respectively, when the period ratio is equal to 1.0. The effects of the chamfered models with taper ratios η = 0% and 2.2% are more significant in decreasing peak dynamic moments when period ratio is equal to 0.95, and the decreased values are up to 67.47% and 81.35%, respectively. This indicates that chamfered modification has better aerodynamic performance and vibration reduction effect. Moreover, contrary to the model without chamfered modification, the peak dynamic moments of chamfered models are not sensitive to the natural period within a certain range because the resonant component of response does not produce a decisive effect on the overall response. Comprehensive analysis and comparisons of the advantages of chamfered modification in corners are discussed in Sect. 3.4.

3.3 Local aerodynamic strategy for reducing loading

Local aerodynamic strategies that opening ventilation slots in the corner of equipment and refuge floors of models A, B, C, and D have been taken. Only the results of model C (η = 2.2%) and D (η = 2.2%, chamfered modification) are shown in this paper, because the mitigation effect of local aerodynamic strategies is the same for η = 0% models and η = 2.2% models.

3.3.1 Local across-wind aerodynamic loads

Fig. 17 shows the effects of various local aerodynamic strategies on σ_{F_y} for non-chamfered model C and chamfered model D. The values of σ_{F_y} of model C (η = 2.2%) initially increase, and then drop along the height when all ventilation slots are closed, and the maximum value of σ_{F_y}

takes place at the upper middle part of the building. The local aerodynamic strategies for different heights have different effects in reducing the values of σ_{F_y}. The effect is the greatest when all ventilation slots are open. The values of σ_{F_y} vary slightly above 0.6 H of the building when S3 is only open; thus, opening S3 is the worst local aerodynamic strategy. Opening S1 or S2 is a better strategy, and the local aerodynamic strategy of opening S1 is more effective than opening S2. However, the reducing effect of local aerodynamic strategies on chamfered model D is less than that on the non-chamfered model C, because chamfered modification removes most of the spectral energy associated with vortex shedding. For example, for non-chamfered model C (η = 2.2%), the values of σ_{F_y} in the ninth pressure tap level for opening all ventilation slots is decreased by 20.2% than that of closing all ventilation slots. Although for chamfered model D (η = 2.2%, chamfered), the values of σ_{F_y} is only decreased by 10.4%, the modification is still highly effective for wind resistance design. In general, for chamfered models, the opening all ventilation slots is the most effective, followed by the opening of S1 or S2, and the effect of opening S3 is the worst. This rule is consistent with non-chamfered models.

The coherence function γ, which indicates the correlation of aerodynamic loads in frequency domain, further reveals the mechanism of local aerodynamic strategies. Fig. 18 shows coherence function $\gamma_{7,8}$ between the seventh and eighth pressure tap level for non-chamfered model C and chamfered model D.

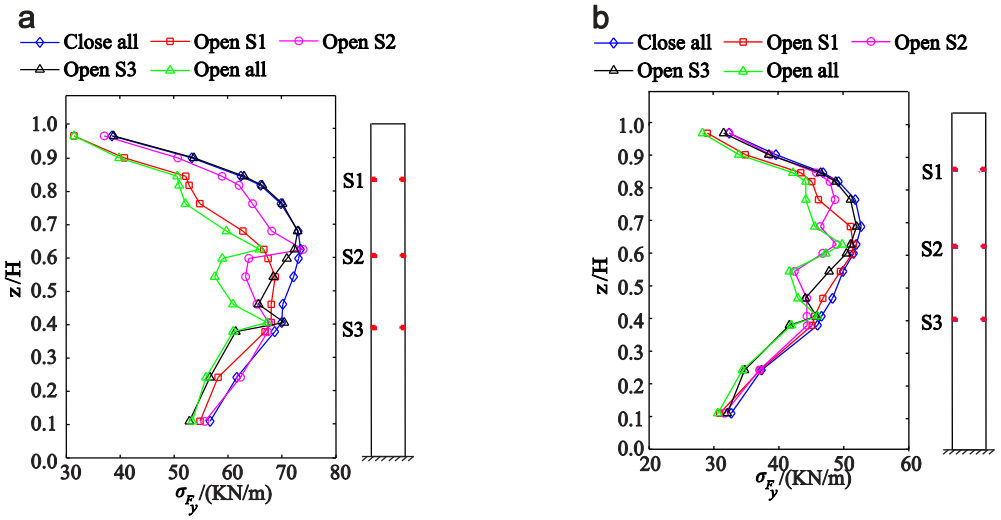

(a) Model C (η = 2.2%) (b) Model D (η = 2.2% chamfered modification)

Fig. 17 Variation of standard deviation of the local cross-wind aerodynamic force of chamfered models with height

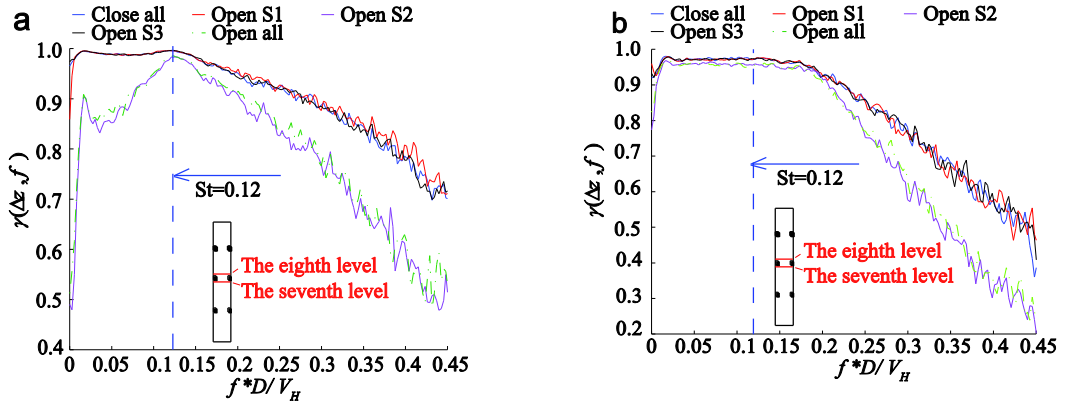

(a) Model C (η = 2.2%) (b) Model D (η = 2.2% chamfered modification)

Fig. 18 Coherence function of cross-wind load between the pressure tap levels seven and eight

S2 is located in the middle of the two pressure tap levels, whose distance Δz is 25 m. It is observed that these coherence functions have similar frequency distribution of energies as the local across-wind aerodynamic forces spectra. The presence of a through-building gap at mid-height of the building is shown to result in some loss of correlation of wind excitations even over the upper half height of the building. The results are consistent with that of To *et al.* (2012). No effect is observed on the correlation when these local aerodynamic strategies are located above the eighth pressure tap level, or below the seventh pressure tap level. However, the value of γ decreases when the local aerodynamic strategy lies between the seventh and eighth pressure tap level, especially in the frequency range that is away from the vortex shedding frequency. The correlation of model D is higher than that of model C in the range below the vortex shedding frequency. In general, the correlation between two pressure tap levels decreases when the local aerodynamic strategies are close to them, and they eventually affect the power spectral density of the base aerodynamic overturning moment.

3.3.2 Base overturning moments and responses

The comparison between power spectral density $S_M(f)$ of the across-wind aerodynamic overturning moments for model C (η = 2.2%) and that for model D (η = 2.2%, chamfered modification) with different local aerodynamic strategies is shown in Fig. 19. Some conclusions are drawn as follows:

- For model C (η = 2.2%), the aerodynamic forces caused by the vortex shedding are remarkable and the spectral energies are concentrated. The local aerodynamic strategies significantly reduce the peak value of $S_M(f)$ at the vortex shedding frequency. The effect of opening all ventilation slots is the best, which is followed by opening S1 and S2, and the effect of opening S3 is the worst.
- For model D (η = 2.2%, chamfered modification), the peak of $S_M(f)$ at the vortex shedding frequency disappears because of chamfered modification. Opening S2 further reduces the power spectra density $S_M(f)$ at the vortex shedding frequency. The effect of opening all

ventilation slots is the best, followed by opening S1 or S2, and the effect of opening S3 is still the worst in this case. Generally, the local aerodynamic strategies conducted on chamfered buildings can still significantly reduce the remaining spectral energy at the vortex shedding frequency.

Further analysis is carried out to compare the performance of different aerodynamic strategies. Fig. 20 shows the power spectral densities of base overturning aerodynamic moment of the models with taper ratio of 0% and 2%. Chamfered modification and opening all ventilation slots after chamfered modification are taken into account. Chamfered modification has a significant effect on the reduction of spectral energy at vortex shedding frequency for models with square cross section, and opening all ventilation slots after chamfered modification is still effective in reducing the remaining spectral energy at vortex shedding frequency.

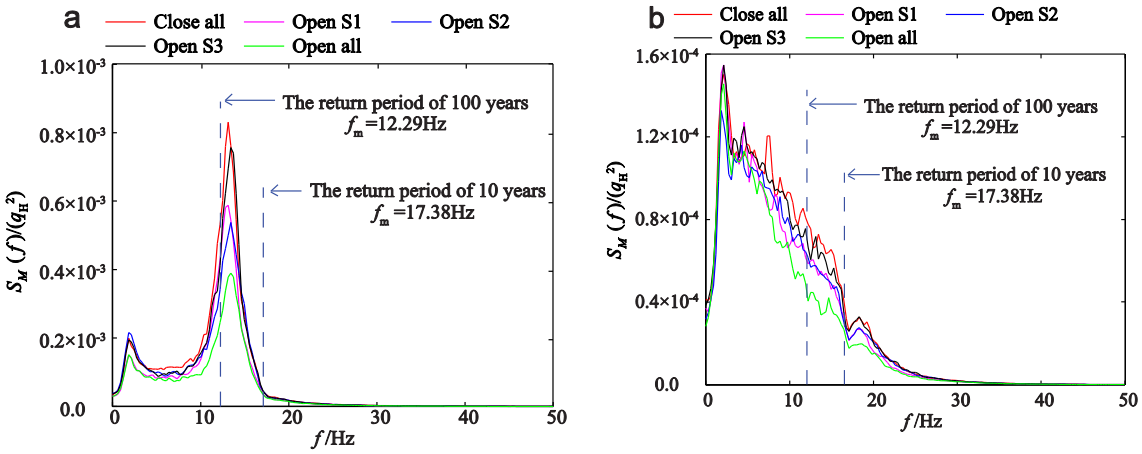

(a) Model C (η = 2.2%) (b) Model D (η = 2.2% chamfered modification)

Fig. 19 Comparison of PSD of base overturning moment

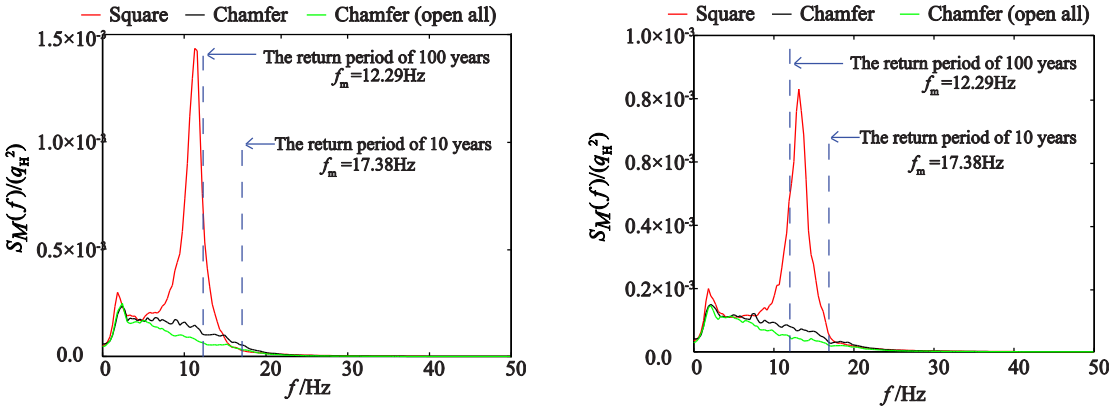

(a) Models with (η = 0%) (b) models with η = 2.2%

Fig. 20 Comparison of PSD of base overturning moment with different aerodynamic strategies

4. Design example

Some super high-rise buildings have applied the local strategies of opening ventilation slots in the corner of equipment and refuge floors. Provided here is the real case of Guangzhou West Tower (GWT) in a typhoon-affected region of Southern China. The height of GWT is 432 m. C category terrain in the loading code for the design of building structures in China (GB5009-2001) was simulated in the wind tunnel. According to the conclusion given in Section 3.3, the mitigation effects of opening S3 located at the range between 0.6 and 0.8 times of the building height and opening all ventilation slots are discussed in a real case. Fig. 21 shows the building elevations and sketches of local aerodynamic strategies.

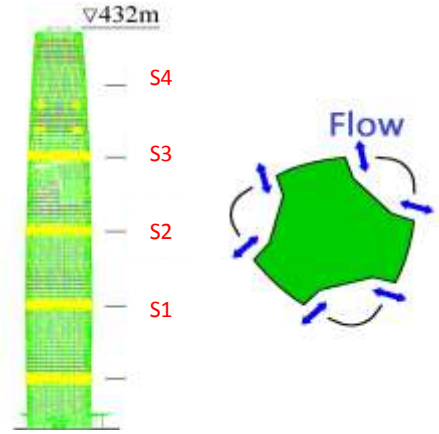

Fig. 21 Building elevations and sketches of local aerodynamic strategies

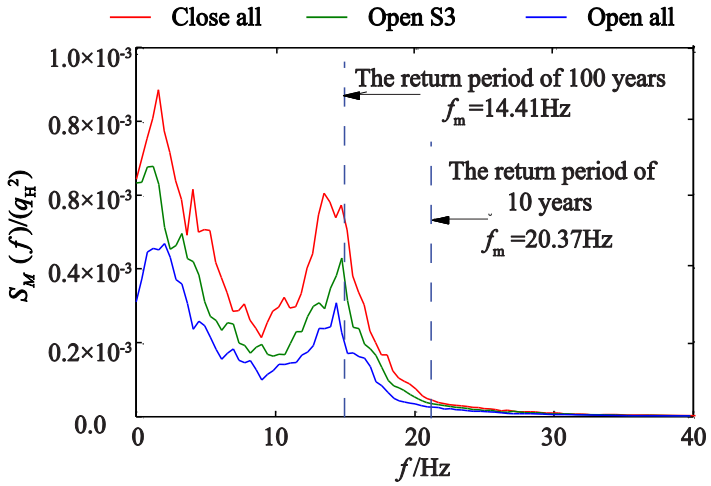

Fig. 22 Comparison of PSD of base overturning moment with different aerodynamic strategies at 120 degrees

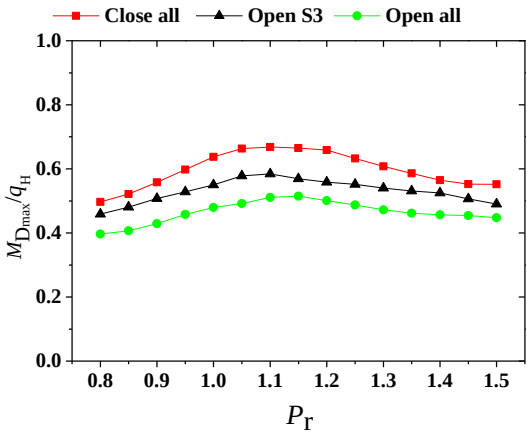

Fig. 23 Reducing vibration effects of different aerodynamic strategies vs. period ratio

Table 2 Effectiveness of local aerodynamic strategies in reducing wind-induced dynamic building responses in actual engineering

Across-wind responses:	Reduction in peak overturning moment	Reduction in peak acceleration
Opening S3	13.7%	10.4%
Opening all S	24.7%	29.4%

Fig. 22 shows the power spectral densities of across-wind base aerodynamic moment of the GWT for different aerodynamic strategies in the most unfavorable wind direction (120 degrees). The high spectral energy distribution at the range below 10.0 Hz is connected to turbulent background. A peak related to vortex shedding occurs at about 14 Hz, and the corresponding St is equal to 0.135. The high St caused by the shape of GWT is detrimental for the wind resistance design. Fig. 22 also shows that the initial natural frequency is close to the vortex shedding frequency at the reduced velocity corresponding to 100-year return period, and it will lead to vortex-induced resonance. Opening S3 or opening all ventilation slots can decrease the value of power spectral densities of base aerodynamic moment at all frequency range, and the effect of opening all ventilation slots is better than that of opening S3. Two kinds of local aerodynamic strategies significantly reduce the value of power spectral densities at the vortex shedding frequency. This shows that local aerodynamic strategies weakened the strength of vortex shedding. The nearer the initial natural frequency approximates to vortex shedding frequency, the better the mitigation effects are. Table 2 shows the mitigation effects of two kinds of local aerodynamic strategies on peak dynamic moment at 100-year return period, and peak acceleration at 10-year return period. The effects of local aerodynamic strategies on reducing wind-induced responses are significant.

Fig. 23 shows the variations in mitigation effects of opening S3 and opening all ventilation slots for GWT with the period ratio Pr. The maximum peak dynamic moment occurs at the period ratio Pr = 1.1, when all ventilation slots are closed. This finding is consistent with the characteristic of power spectral densities of base aerodynamic moment. Opening S3 and opening all ventilation slots reduce the peak dynamic moment by 12.5% and 23.5%, respectively.

5. Conclusions

(1) Changing cross section along with height by tapering can effectively reduce the across-wind aerodynamic loads for super high-rise buildings with standard square cross section. With increased taper ratio η, the mitigation effect becomes greater. At the same time, the vortex shedding frequency increases; this will probably produce a greater response than those buildings with a standard square cross section.

(2) Chamfered modification can evidently suppress the across-wind vortex shedding for a tapered building. The peak dynamic base moments of buildings with taper ratios of 2.2% and 4.4% reduce by up to 73.81% and 80.93%, respectively, in the 100-year return period. Chamfered building with a taper ratio of 2.2% is a recommended option in wind-resistant design of super high-rise buildings, when the building shape and net building area are all taken into account.

(3) For buildings without corner modification, local aerodynamic strategies can significantly reduce the spectra energy of across-wind aerodynamic moments. The residual spectral energy at vortex shedding frequency can also be remarkably weakened by taking local aerodynamic strategies for chamfered buildings. Opening all ventilation slots is the most effective local strategy to reduce the peak dynamic moments corresponding to 100-year return period for buildings C (η = 2.2%) and D (η = 2.2%, chamfered) by 14.1% and 5.8%, respectively. If only one ventilation slot is open, the reduction is better when the local aerodynamic strategy is in the locations whose height ranges from 0.6 to 0.8 times of the building height.

Acknowledgments

The authors would like to gratefully acknowledge the National Natural Science Foundation of China (Grant no. 51278104 and 51078146) and the Fundamental Research Funds for the Central Universities (Grant no. 2015ZM001) for supporting their contribution in this work.

References

Bandi, E.K., Tamura, Y., Yoshida, A., Kim, Y.C. and Yang, Q.S. (2013), "Experimental investigation on aerodynamic characteristics of various triangular-section high-rise buildings", *J. Wind Eng. Ind. Aerod.*, **122**, 60-68.

Davenport, A.G. (1964), "Note on the distribution of the largest value of a random function, with application to gust loading", *Proc. Inst Civ. Engrs.*, **28**, 187-196.

Gu, M. and Quan, Y. (2004), "Across-wind loads of typical tall buildings", *J. Wind Eng. Ind. Aerod.*, **92**(13), 1147-1165.

Hayashida, H. and Iwasa, Y. (1990), "Aerodynamic shape effects of tall building for vortex induced

vibration", *J. Wind Eng. Ind. Aerod.*, **33**(1-2), 237-242.
Kawai, H. (1998), "Effect of corner modifications on aeroelastic instabilities of tall buildings", *J. Wind Eng. Ind. Aerod.*, **74-76**, 719-729.
Kim, Y.C. and Kanda, J. (2010), "Characteristics of aerodynamic forces and pressures on square plan buildings with height variations", *J. Wind Eng. Ind. Aerod.*, **98**(8-9), 449-465.
Kim, Y.C. and Kanda, J. (2015), "Effects of taper and set-back on wind force and wind-induced response of tall buildings", *Wind Struct.*, **13**(6), 499-517.
Kim, Y.C., Tamura, Y. and Yoon, S.W. (2015), "Effect of taper on fundamental aeroelastic behaviors of super-tall buildings", *Wind Struct.*, **20**(4), 527-548.
Kim, Y.M. and You, K.P. (2002), "Dynamic response of a tapered tall building to wind loads", *J. Wind Eng. Ind. Aerod.*, **90**(12-15), 1771-1782.
Kim, Y.M., You, K.P. and Ko, N.H. (2008), "Across-wind responses of an aeroelastic tapered tall building", *J. Wind Eng. Ind. Aerod.*, **96**(8-9), 1307-1319.
Miyashita, K. and Katagiri, J. (1993), "Wind-induced response of high-rise buildings", *J. Wind Eng. Ind. Aerod.*, **50**, 319-328.
Solari, G. (1996), "Evaluation and role of damping and periods for the calculation of structural response under wind loads", *J. Wind Eng. Ind. Aerod.*, **59**, 191-210.
Tamura, T. and Miyagi, T. (1999), "The effect of turbulence on aerodynamic forces on a square cylinder with various corner shapes", *J. Wind Eng. Ind. Aerod*., **83**(1-3), 135-145.
Tamura, Y. and Suganuma, S. (1996), "Evaluation of amplitude-dependent damping and natural frequency of buildings during strong winds", *J. Wind Eng. Ind. Aerod.*, **59**, 115-130.
Tanaka, H. and Tamura, Y., Ohtake, K., Nakai, M. and Kim, Y.C. (2012), "Experimental investigation of aerodynamic forces and wind pressures acting on tall buildings with various unconventional configurations", *J. Wind Eng. Ind. Aerod*., **107-108**, 179-191.
To, A.P., Lam, K.M., Wong, S.Y. and Xie, Z.N. (2012), "Effect of a through-building gap on wind-induced loading and dynamic responses of a tall building", *Wind Struct.*, **15**(6), 531-553.
Tse, K.T., Hitchcock, P.A., Kwok, K.C.S., Thepmongkorn, S. and Chan, C.M. (2009), "Economic perspectives of aerodynamic treatments of square tall buildings", *J. Wind Eng. Ind. Aerod.*, **97**(9-10), 455-467.
Xie, J.M. (2014), "Aerodynamic optimization of super-tall buildings and its effectiveness assessment", *J. Wind Eng. Ind. Aerod.*, **130**, 88-98.
You, K.P., Kim, Y.M. and Ko, N.H. (2008), "The evaluation of wind-induced vibration responses to a tapered tall building", *J. Wind Eng. Ind. Aerod.*, **17**(3), 655-667.

JH